Optical excitation and detection of neuronal activity

Chenfei Hu[1,6], Richard Sam[2,6], Mingguang Shan[6,7], Viorel Nastasa[6,8,#], Minqi Wang[2,6], Taewoo Kim[1,6,†], Martha Gillette[3,4,5,6], Parijat Sengupta[3,5,6], and Gabriel Popescu[1,3,6,]*

1) Department of Electrical and Computer Engineering,
2) School of Molecular and Cellular Biology,
3) Department of Bioengineering,
4) Department of Cell and Developmental Biology,
5) Neuroscience Program,
6) Beckman Institute for Advanced Science and Technology,
University of Illinois at Urbana-Champaign, Urbana, Illinois 61801, USA
7) College of Information and Communication Engineering,
Harbin Engineering University, Harbin, Heilongjiang 150001, China
8) National Institute for Laser Plasma and Radiation Physics, Magurele, Ilfov 077125, Bucharest, Romania

†Currently with Caltech Optical Imaging Laboratory, California Institute of Technology, Pasadena, CA, 91125, USA.

Currently at Extreme Light Infrastructure - Nuclear Physics/ Horia Hulubei National Institute for R&D in Physics and Nuclear Engineering, 30 Reactorului Street, 077125 Magurele, Ilfov, Romania

*Corresponding author: gpopescu@illinois.edu

ABSTRACT

Optogenetics has emerged as an exciting tool for manipulating neural activity, which in turn, can modulate behavior in live organisms. However, detecting the response to the optical stimulation requires electrophysiology with physical contact or fluorescent imaging at target locations, which is often limited by photobleaching and phototoxicity. In this paper, we show that phase imaging can report the intracellular transport induced by optogenetic stimulation. We developed a multimodal instrument that can both stimulate cells with high spatial resolution and detect optical pathlength changes with nanometer scale sensitivity. We found that optical pathlength fluctuations following stimulation are consistent with active organelle transport. Furthermore, the results

indicate a broadening in the transport velocity distribution, which is significantly higher in stimulated cells compared to optogenetically inactive cells. It is likely that this label-free, contactless measurement of optogenetic response will provide an enabling approach to neuroscience.

Introduction

Optogenetics is a transforming tool in the field of neuroscience. By genetic engineering, a neuron can express light-sensitive proteins, and its activity can be initiated or inhibited using light. For example, delivering light stimulation on *opsin* family proteins causes changes in the cation level, which can trigger or prevent action potentials [1]. Unlike electrical stimulation, light stimulation manipulates specific neurons, and makes it possible to investigate the role of subpopulation neurons in a neural circuit [2]. Over the past decade, accompanied by advances in virus targeting methods (*i.e.*, adeno-associated virus), as well as novel light delivery mechanisms (e.g., two-photon excitation combined with spatial light modulation), the optogenetics toolbox has been growing and gradually becoming a standard method for studying neural functions at both the cellular and behavioral level [2-5].

Currently, electrophysiological methods are considered to provide the highest fidelity readout of neural activity, which is essentially achieved by attaching physical electrodes to the sample [6]. Though these approaches offer high sensitivity, they require physical contact and cell impaling, while the throughput is low. Recent developments in micro-electrode arrays allows for a simultaneous recording of up to a few hundred neurons [2]. Unfortunately, the low spatial resolution, lack of control over the excitation, and photoelectric effects induced in the electrode by the process of stimulation are inevitable limitations [7]. Optical imaging is a potential solution for circumventing these limitations of electrophysiology. This is typically realized by introducing exogenous fluorescent labels or sensors that change their properties when cells are activated [8, 9]. However, the process requires careful sample preparation and is often toxic to cells [10].

Recently, quantitative phase imaging (QPI) [11] has emerged as a valuable tool for live cell imaging, especially because it is label-free and nondestructive. QPI relies on the principle of

interference, whereby an image field is overlaid with a reference field. As a result, even the most transparent objects, such as unlabeled live cells, can be imaged with high contrast and sensitivity using the phase information of the field. Because the phase of the image field is measured quantitatively, it can report on both the thickness and dry mass density of the specimen. A number of methods have been proposed, especially over the past 1-2 decades, to optimize the following properties: spatial and temporal resolution, spatial and temporal sensitivity [12-16]. With the recent advances, QPI has become a significant method for studying live cells, such as red blood cell dynamics [17-20], cell growth [21, 22], cell dynamics [23-26] and cell tomography [27-29]. Using its multi-scale coverage and high sensitivity to sub-nanometer changes in optical pathlength, QPI has also found applications in neuroscience and enabled non-invasive studies of neurons at both single-cell level and network level [30-32].

In this paper, we present a new instrument that is capable of both exciting optogenetic signals and detecting the cell response using interferometry. The overall optical pathlength sensitivity is 1.1 nm. We demonstrate that the optical pathlength signals measured via QPI reports on neurite transport associated with optogenetically activated PC12-derived neurons. The new approach for measuring the neural response to stimulation, without labels or physical contact, combines a high spatial resolution optogenetic stimulation system with a high-sensitivity quantitative phase imaging instrument.

Results

The experimental setup is shown in Fig. 1. We use a commercial inverted microscope (Axio Observer Z1, Zeiss) onto which we attach the excitation and detection modules. In order to achieve single cell level resolution and selectivity in excitation wavelength, we use a high power

commercial projector (Epson Home Cinema 5030UB). The epi-fluorescence excitation source of the commercial microscope is replaced with the commercial projector, which forms an image of the projected pattern on the sample plane via the collector lens (Lens 3) and brightfield objective lens (40X, NA=0.75). This lens system demagnifies the image by a factor of 10, such that a single projector pixel has a dimension around 0.8 μm at the sample plane. The diffraction limited image of this excitation pattern is relayed by the microscope to the camera plane, via the reflection optical path.

Figure 1b illustrates an excitation dot at blue wavelength, which is projected onto a live neuron. Simultaneously, on the transmission path, we built a phase sensitive interferometric system, known as the diffraction phase microscopy (DPM). This system is described in more detail elsewhere [33-35]. Briefly, at the image plane of the microscope, we place a diffraction grating, which splits the imaging field into multiple diffraction orders. All the diffraction orders are blocked, except for the 0th and 1st order. These two beams form an off-axis common-path Mach-Zehnder interferometer, in which Lenses 1-2 form a 4f system that images the grating at the camera plane. In order to obtain a reference field for the interferometer, we spatially filter the 0th order through a pinhole at the Fourier plane of Lens 1. The 1st order is passed without filtering and carries full information (i.e., amplitude and phase) about the image field. The spatial filter is achieved by an amplitude Spatial Light Modulator (SLM), onto which we write a binary mask of maximum (white) and minimum (black) transmission, as shown in Fig. 1c.

The camera records an interferogram of the form

$$I(x,y) = I_0 + I_1 + 2\sqrt{I_0 I_1}\cos\left[\varphi(x,y) + \alpha x\right] \qquad [1]$$

Where I_0 and I_1 are the intensities of the (filtered) 0th and 1st order, respectively, φ is the phase map of the object and α is the spatial modulation frequency, $\alpha = 2\pi/\Lambda$, with Λ the period of the grating. Ensuring proper sampling (see Ref [35] for details), the quantitative phase map is obtained via a Hibert transform [35]. We chose the DPM system for our phase imaging because it is common-path, thus, highly stable, and also provides high-throughput due to its single shot performance. Moreover, using a LED as a white-light source with low temporal coherence, this system minimizes the speckle noise that can degrade the sensitivity of the phase imaging system [34]. Figure 1d illustrates an interferogram associated with a live neuron. The three spectral bands of the projectors are shown in Fig. 1e. To eliminate the overlap between the three channels, we used a 450 nm band-pass and a 610 nm long pass filters, respectively. The blue channel was used for excitation and the red for control.

Figure 2 shows the phase reconstruction procedure and the noise characteristic of the DPM system. An implementation of spatial Hilbert transform takes the input interferogram (Fig. 2a), performs a Fourier transform (Fig. 2b), selects only one side of the Fourier spectrum (red continuous circle in Fig. 2b), shifts this selection to the center of the image (dotted circle in Fig. 2b), and Fourier transform this signal back to the spatial domain, where the argument provides the phase map, φ (Fig. 2c).

In order to assess the stability of our instrument, which in turn, governs the spatiotemporal optical pathlength sensitivity, we recorded a time series of ‘no sample’ images (inset of Fig. 2d). Figure 2a shows the raw interferogram recorded at the camera, while Fig. 2b illustrates the associated Fourier spectrum and Fig. 2c the resulting phase map. The temporal standard deviation was calculated at each point in the field of view. The histogram of these values is shown in Fig. 2d and the standard deviation of the distribution is shown to be 1.13 nm.

We applied our excitation-detection composite system to live PC12 differentiated neuron-like cells that were optogenetically active. The transfection protocol is described in Materials and Methods. Due to the low transfection rate, we used a Red Fluorescent Protein (RFP) reporter, mCherry, to identify the optogenetically active cells (Fig. 3a). We performed DPM imaging before and after blue light stimulation, as well as after red light excitation (Figs 3b-c). The imaging procedure is described further in Methods. The DPM time lapse was acquired at 5 frames/s for a duration of 180 seconds. To observe in detail the dynamic changes associated with the optogenetic excitation, we plot the optical pathlength along a segment of a dendrite vs. time (Fig. 3c). The measurements indicated that there is clear increase under blue light excitation. This behavior is absent before the excitation and after red light excitation. Note that the pathlength change that follows the excitation is very subtle, of the order of 10-20 nm, which will be undetectable under a conventional, intensity-based microscope. Blue light stimulation results in the opening of the optogenetic channel ChR2, which allows positive ions like calcium, potassium, sodium and hydrogen to enter the cell from the extracellular medium. The sudden influx of positive ions depolarizes the cell, and this can trigger the transport of various cellular organelles, including vesicles, mitochondria and peroxisomes. This increase in optical path length, or local dry mass, is likely due to organelle transport that is associated with the ion influx[36].

Using this procedure, we analyzed 9 regions of interest (ROI) of 5 active and 7 inactive neurons, respectively. The results are summarized in Fig. 3d-e, where we plot the magnitude of the optical pathlength difference with respect to the frame at t=0. Clearly, we obtain a significant signal only for active neurons after excitation with blue light. These findings validate the conclusion that our method is capable of sensing nanometer scale changes in optical pathlength associated with the optogenetic activity.

In order to quantify intracellular mass transport, we applied dispersion-relation phase spectroscopy (DPS) [23, 30, 37]. This approach allows us to analyze time-resolved phase maps and extract information about the nature of mass transport, namely, diffusive or deterministic. From the image stack, we compute a temporal bandwidth, Γ, at each spatial frequency, q (see Supplemenatl Information for details of the computation). Modeling the intracellular transport by a diffusion-advection equation, the dispersion relation satisfies

$$\Gamma(q) = \Delta v q + D q^2, \qquad [2]$$

where Δv is the width of the velocity distribution and D is the diffusion coefficient. Thus, by fitting the data with Eq. 2, we can infer both Δv and D.

We applied DPS to subcellular regions before and after excitation with both red and blue light and in the absence of stimulation. Figure 4a-d illustrates this analysis for one active and one inactive cell. On the ROIs containing dendrites or axons, the data shows that deterministic transport (*i.e.*, linear Γ vs. q curve) is dominant in all cases as expected. However, upon blue stimulation, there is a 35.8% increase in the Δv value, compared with the value under the condition of no stimulation. This increase is indicative of a high probability for faster transport, irrespective of the velocity direction. This result is consistent with those we obtained in Figs 3-4. Measuring a dominant deterministic (directed, active) transport is consistent with previous reports on traffic along dendrites [38].

Figure 4e summarizes the Δv measurements obtained from 12 regions in 5 active and 7 inactive cells. We found that the optogenetic excitation is accompanied by a change in Δv value of 25% on average. This change in Δv with respect to the red excitation control case is statistically

significant as evidenced by a p-value of 0.0043. This result again indicates that there is an active transport associated with the light stimulation.

Materials and Methods:

1. *Cell imaging*

Throughout imaging, neurons were set on a heated stage enclosed with an incubator (Zeiss), which maintained an atmosphere of 37 °C and 5% CO_2. For one neuron cell, the imaging was repeated 3 times, with each under a different light excitation condition: no stimulation, red light (~650 nm) and blue light (~460 nm), in this order. The stimulation lasted for 3 seconds, and DPM measurement was immediately followed in the next 3 minutes, at a speed of 5 frames/second. The current system provides light power of 0.31 mW/mm^2. Considering the long exposure time, the power exerted on the cells should be enough to activate the ion channels [39]. To minimize correlation between different excitation, a time interval around 5-7 minutes was set between two consecutive measurements. The experiment was conducted in a dark room, and cells were only exposed to the light in the process of stimulation, imaging and observing fluorescent signal.

2. *Neuron preparation*

PC12 cells were maintained in RPMI (Roswell Park Memorial Institute) medium supplemented with 10% horse serum and 5% fetal bovine serum in 5% CO_2 at 37ºC. Samples were prepared on dishes coated with PDL and Fibronectin. Cells were nucleofected with pCAG-ChR2 with mCherry tag and plated. After plating, NGF was added (Nerve Growth Factor, 100ng/ml) into RPMI supplemented with 10% horse serum, 5% fetal bovine serum, and 1% Penstrep. Cells were

incubated at 37ºC at 5% CO_2 to induce differentiation into neurons. The PC12 differentiated neurons were incubated for at least 7 days before imaging.

3. *Dispersion-relation Phase Spectroscopy (DPS)*

Dispersion-relation Phase Spectroscopy (DPS) characterizes the nature of mass transport (i.e. deterministic transport and diffusion) without tracking individual particles. Figure 5 summarizes the DPS procedure. Because a phase map, φ, is essentially proportional to dry mass density, it is assumed to satisfy the diffusion-advection equation, namely[23]

$$D\nabla^2\varphi(\boldsymbol{r},t)-\boldsymbol{v}\cdot\nabla\varphi(\boldsymbol{r},t)-\frac{\partial}{\partial t}\varphi(\boldsymbol{r},t)=0 \qquad [3]$$

where $\boldsymbol{r}$ the spatial coordinates, D the diffusion coefficient, $\boldsymbol{v}$ the advection velocity. Taking a Fourier transform with respect to $\boldsymbol{r}$, we obtain the expression in frequency domain

$$\left(-Dq^2+i\boldsymbol{q}\cdot\boldsymbol{v}-\frac{\partial}{\partial t}\right)\varphi(\boldsymbol{q},t)=0 \qquad [4]$$

In Eq. 4, we use the same symbols with different argument for a function and its Fourier transform, i.e., $f(\boldsymbol{r})\leftrightarrow f(\boldsymbol{q})$, where f is an arbitrary signal and $\leftrightarrow$ indicates the Fourier transform. Following the calculation in Ref. 23, the temporal autocorrelation, g, at each spatial frequency can be modeled as

$$g(q,\tau)=e^{i\boldsymbol{v}_0\bullet\boldsymbol{q}\tau}e^{-q\Delta v\tau-Dq^2\tau} \qquad [5]$$

Here, $\boldsymbol{v}_0$ represents the mean velocity, and it is considered negligible, and a digital registration is also performed on each image stack to minimize shifting between frames. Thus, we obtain the exponentially decay rate at each spatial frequency $\Gamma(q)$ as seen in Eq. 2. And Γ is the standard

deviation of the spatial power spectrum (Fig.5 d). A radial average is performed to compress the 2D map into 1D line profile (Fig. 5e). The Δv and D is then extracted by fitting the data to Eq. 2.

Data availability

The data that support the findings of this study are available from the corresponding author upon reasonable request.

Summary and discussion:

In summary, we developed a multimodal instrument that allows for both optogenetic stimulation and detection. This stimulation module exploits computer projection to achieve subcellular spatial resolution and multicolor channel. The detection path consists of a highly sensitive phase imaging system, which provides sensitivity to optical pathlength changes on the order of 1 nm.

We studied optogenetically active neurons that were excited with blue light and, as negative control, we imaged cells illuminated with red light as well as optogenetically inactive neurons. We found a consistent increase in cellular dry mass fluctuations, or optical pathlength, for the optogenetically excited group. Detailed analysis of the physical nature of these fluctuation reveals a dispersion relation that is consistent with deterministic organelle transport initiated by the optical stimulation. Furthermore, the value of the change in the velocity distribution standard deviation is significantly higher in the stimulated neurons, suggesting an increase in directed transport. Together, these findings indicate that the organelle transport that accompanies the stimulation can be detected without labels or physical contact using quantitative phase imaging. Because our composite instrument can be attached to an existing microscope, we anticipate that it will be broadly adopted by the neuroscience community.

Acknowledgement:

We gratefully appreciated the funding support from National Science Foundation (NSF) STC CBET 0939511, NSF BRAIN EAGER DBI 1450962, and IIP-1353368.

Author Contributions:

M.G., P.S., and G.P. proposed the project. T.K., M.S., and V.N. built the excitation module. C.H. and M.S built the DPM system. M.W. prepared DNA. R.S. prepared cell samples. C.H. performed quantitative phase imaging and data analysis. G.P. and P.S. supervised the research. C.H and G.P. wrote the manuscript.

Competing financial interest:

G.P. has financial interest in Phi Optics, Inc., a company developing quantitative phase imaging technology for materials and life science applications.

Reference:

1. Yizhar, O., et al., *Optogenetics in neural systems.* Neuron, 2011. **71**(1): p. 9-34.
2. Packer, A.M., B. Roska, and M. Hausser, *Targeting neurons and photons for optogenetics.* Nat Neurosci, 2013. **16**(7): p. 805-15.
3. Busskamp, V., et al., *Genetic reactivation of cone photoreceptors restores visual responses in retinitis pigmentosa.* Science, 2010. **329**(5990): p. 413-7.
4. Packer, A.M., et al., *Two-photon optogenetics of dendritic spines and neural circuits.* Nat Methods, 2012. **9**(12): p. 1202-5.
5. Fenno, L., O. Yizhar, and K. Deisseroth, *The development and application of optogenetics.* Annu Rev Neurosci, 2011. **34**: p. 389-412.
6. Scanziani, M. and M. Hausser, *Electrophysiology in the age of light.* Nature, 2009. **461**(7266): p. 930-939.
7. Cardin, J.A., et al., *Targeted optogenetic stimulation and recording of neurons in vivo using cell-type-specific expression of Channelrhodopsin-2.* Nat. Protocols, 2010. **5**(2): p. 247-254.
8. Akerboom, J., et al., *Genetically encoded calcium indicators for multi-color neural activity imaging and combination with optogenetics.* Front Mol Neurosci, 2013. **6**: p. 2.
9. Guo, Z.V., A.C. Hart, and S. Ramanathan, *Optical interrogation of neural circuits in Caenorhabditis elegans.* Nat Methods, 2009. **6**(12): p. 891-6.
10. Jensen, E.C., *Use of Fluorescent Probes: Their Effect on Cell Biology and Limitations.* Anatomical Record-Advances in Integrative Anatomy and Evolutionary Biology, 2012. **295**(12): p. 2031-2036.
11. Popescu, G., *Quantitative phase imaging of cells and tissues*. McGraw-Hill biophotonics. 2011, New York: McGraw-Hill. xx, 362 p.
12. Wang, Z., et al., *Spatial light interference microscopy (SLIM).* Optics Express, 2011. **19**(2): p. 1016-1026.
13. Edwards, C., et al., *Epi-illumination diffraction phase microscopy with white light.* Optics Letters, 2014. **39**(21): p. 6162-6165.
14. Chowdhury, S., et al., *Structured illumination multimodal 3D-resolved quantitative phase and fluorescence sub-diffraction microscopy.* Biomed Opt Express, 2017. **8**(5): p. 2496-2518.
15. Park, Y., et al., *Diffraction phase and fluorescence microscopy.* Opt Express, 2006. **14**(18): p. 8263-8.
16. Ikeda, T., et al., *Hilbert phase microscopy for investigating fast dynamics in transparent systems.* Optics Letters, 2005. **30**(10): p. 1165-1167.
17. Park, Y.K., et al., *Metabolic remodeling of the human red blood cell membrane.* Proceedings of the National Academy of Sciences of the United States of America, 2010. **107**(4): p. 1289-1294.
18. Bhaduri, B., et al., *Optical assay of erythrocyte function in banked blood.* Sci Rep, 2014. **4**: p. 6211.
19. Lee, K., et al., *Quantitative phase imaging techniques for the study of cell pathophysiology: from principles to applications.* Sensors (Basel), 2013. **13**(4): p. 4170-91.
20. Rinehart, M.T., et al., *Hemoglobin consumption by P. falciparum in individual erythrocytes imaged via quantitative phase spectroscopy.* Sci Rep, 2016. **6**: p. 24461.
21. Mir, M., et al., *Optical measurement of cycle-dependent cell growth.* Proceedings of the National Academy of Sciences of the United States of America, 2011. **108**(32): p. 13124-13129.
22. Mir, M., et al., *Highly sensitive quantitative imaging for monitoring single cancer cell growth kinetics and drug response.* PLoS One, 2014. **9**(2): p. e89000.
23. Wang, R., et al., *Dispersion-relation phase spectroscopy of intracellular transport.* Opt Express, 2011. **19**(21): p. 20571-9.

24. Eldridge, W.J., et al., *Imaging deformation of adherent cells due to shear stress using quantitative phase imaging.* Optics Letters, 2016. **41**(2): p. 352-355.
25. Kemper, B. and G. von Bally, *Digital holographic microscopy for live cell applications and technical inspection.* Applied Optics, 2008. **47**(4): p. A52-A61.
26. Eldridge, W.J., et al., *Optical Phase Measurements of Disorder Strength Link Microstructure to Cell Stiffness.* Biophysical Journal, 2017. **112**(4): p. 692-702.
27. Kim, T., et al., *White-light diffraction tomography of unlabelled live cells.* Nat Photon, 2014. **8**(3): p. 256-263.
28. Choi, W., et al., *Tomographic phase microscopy.* Nature methods, 2007. **4**(9): p. 717.
29. Cotte, Y., et al., *Marker-free phase nanoscopy.* Nature Photonics, 2013. **7**(2): p. 113-117.
30. Mir, M., et al., *Label-free characterization of emerging human neuronal networks.* Sci Rep, 2014. **4**: p. 4434.
31. Kandel, M.E., et al., *Three-dimensional intracellular transport in neuron bodies and neurites investigated by label-free dispersion-relation phase spectroscopy.* Cytometry A, 2017.
32. Lee, Y.J., et al., *Quantitative assessment of neural outgrowth using spatial light interference microscopy.* Journal of Biomedical Optics, 2017. **22**(6): p. 066015-066015.
33. Popescu, G., et al., *Diffraction phase microscopy for quantifying cell structure and dynamics.* Opt Lett, 2006. **31**(6): p. 775-7.
34. Bhaduri, B., et al., *Diffraction phase microscopy with white light.* Opt Lett, 2012. **37**(6): p. 1094-6.
35. Bhaduri, B., et al., *Diffraction phase microscopy: principles and applications in materials and life sciences.* Advances in Optics and Photonics, 2014. **6**(1): p. 57-119.
36. van Bergeijk, P., et al., *Optogenetic control of organelle transport and positioning.* Nature, 2015. **518**(7537): p. 111-+.
37. Cintora, P., et al., *Cell density modulates intracellular mass transport in neural networks.* Cytometry A, 2017. **91**(5): p. 503-509.
38. Wang, R., et al., *One-dimensional deterministic transport in neurons measured by dispersion-relation phase spectroscopy.* J. Phys.: Cond. Matter, 2011. **23**: p. 374107.
39. Grossman, N., et al., *Multi-site optical excitation using ChR2 and micro-LED array.* Journal of Neural Engineering, 2010. **7**(1).

Figure Captions:

1. System Schematic. (a) white-light Diffraction Phase Microscopy (wDPM) system combines a projector to achieve spatially-resolved optical stimulation and label-free imaging. (b) Stimulation pattern, a disk of 21 μm in diameter. (c) SLM mask. (d) Raw image of a neuron cell, and the dashed circle indicates the position and size of the stimulation spot. (e) Spectrum of blue, red light stimulation, and fluorescent excitation measured at the sample plane.

2. Procedure of phase reconstruction. (a) a raw image which is an interference between reference and 1st order diffraction, the zoom-in image shows the fringes. (b) Fourier transform of the raw image, one of the sidelobes is isolated and then moved to the image center. (c) an optical pathlength (OPL) map is reconstructed after taking inverse Fourier transform, background subtraction and halo removal (unit in nm). (d) Histogram of spatiotemporal noise with a standard deviation of 1.13 nm, the inset represents a time stack images of system noise.

3. (a) One fluorescent image of an ChR2 active neuron and (b) its corresponding quantitative phase image with units in OPL. (c) The mass density steadily increased along this active cell dendrite after stimulation with blue light. (d-e) OPL change after different stimulation on both ChR2+ and ChR2- neurons. 9 different ROIs with a size of 30×30 pixels across 5 ChR2 active neurons and 7 ChR2 negative neurons were selected, respectively. All ROIs were located either on neuron dendrites, axon, or the region of cellbody close to a dendrite. The absolute change of averaged phase with respect to t=0 were plotted for each stimulation condition, with standard errors in light-gray lines.

4. DPS analysis were performed on one ChR2 positive (a-c) and ChR2 negative(c-d) neuron at selected region indicated by a red box for each stimulation condition. (e) Box chart of the transport velocity change compared with the velocity under no light stimulation after different stimulation on ChR2+ and ChR2- (unit in %). A total of 12 ROIs were selected in both active and negative neurons, respectively.

5. Procedure of DPS analysis. (a) A region of interest (ROI) in the field of view is selected, and (b) the image volume is digitally aligned to minimize drifts between frames. (c) Taking a Fourier transform on each frame, (d) the temporal bandwidth is then evaluated and obtain map of Γ. (e) Performing a radial average on (d) and present in a log plot, the advection and diffusion coefficients are extracted from dispersion curve.

Figures:

1.

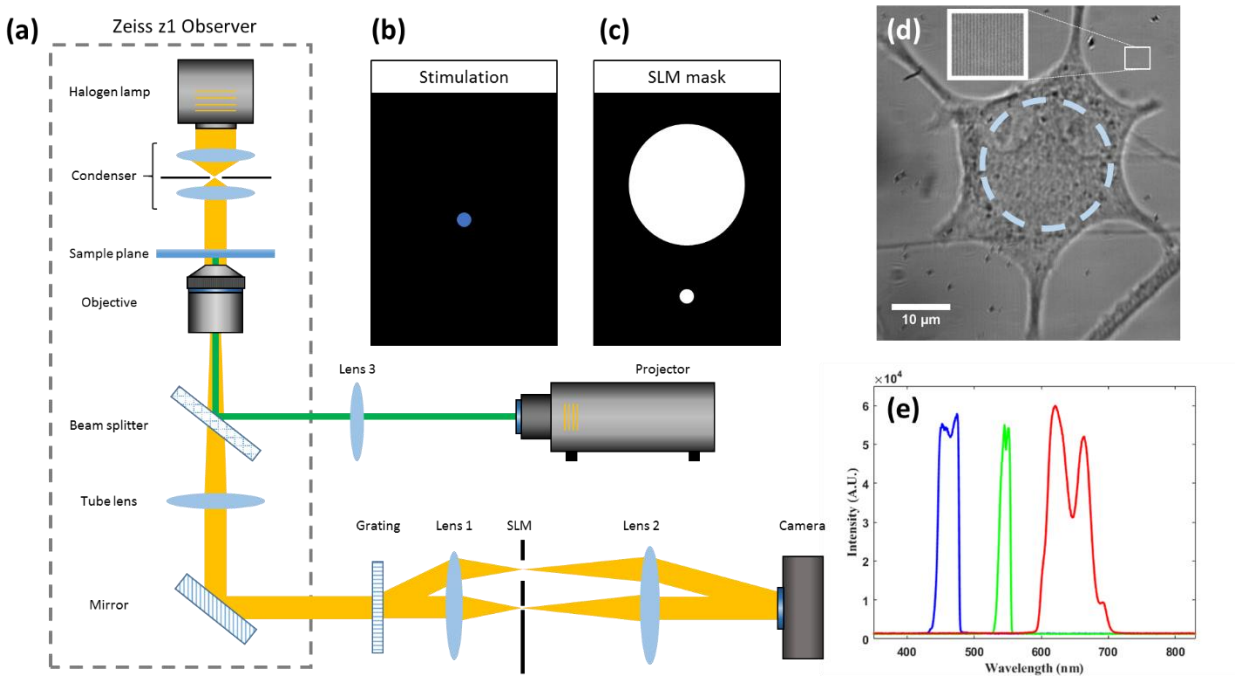
(a)
Zeiss z1 Observer
Halogen lamp
Condenser
Sample plane
Objective
Beam splitter
Tube lens
Mirror
(b)
Stimulation
(c)
SLM mask
Lens 3
Projector
Grating
Lens 1
SLM
Lens 2
Camera
(d)
10 µm
(e)
×10^4
Intensity (A.U.)
Wavelength (nm)

2.

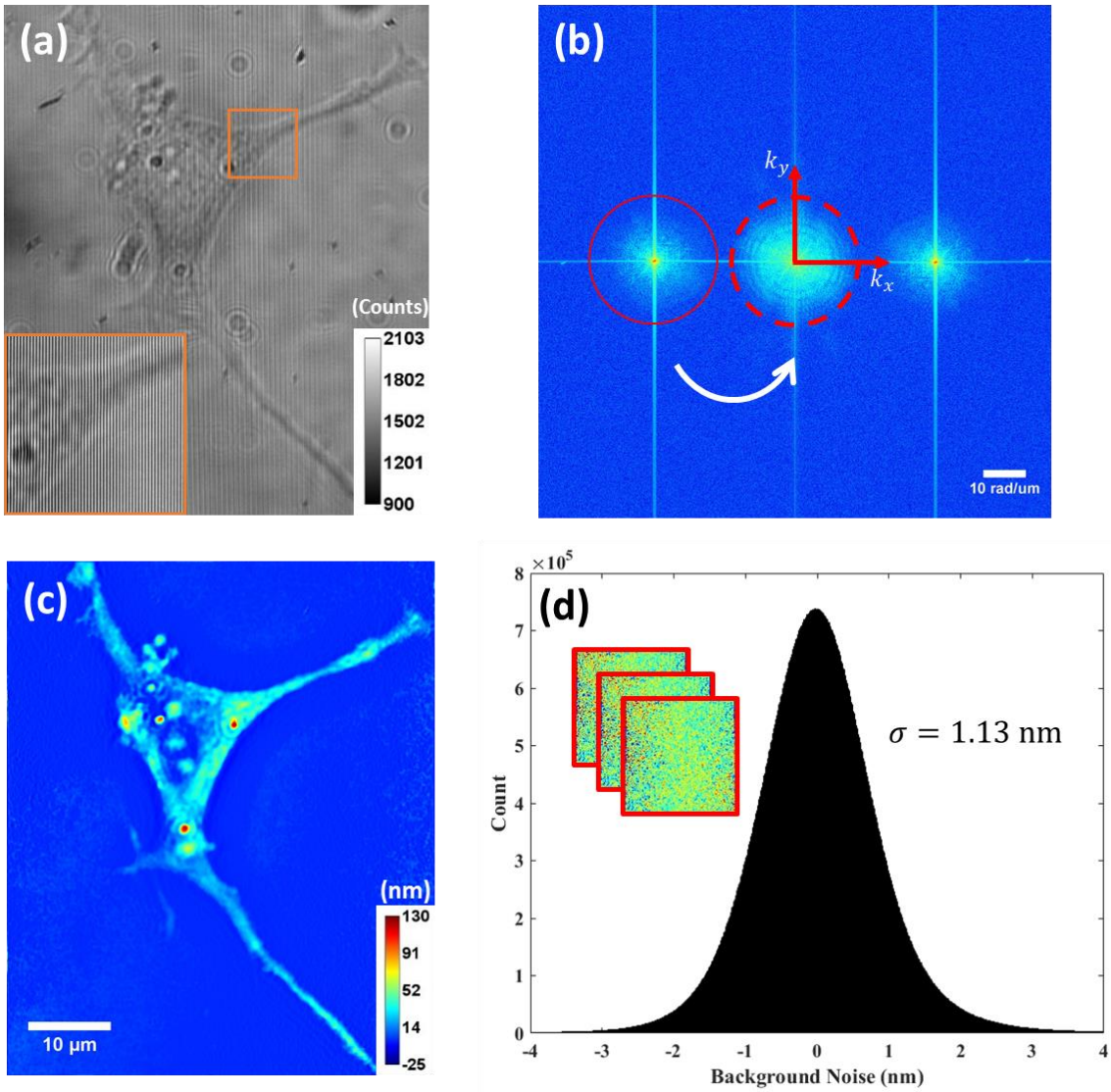
(a)
(Counts)
2103
1802
1502
1201
900
(b)
k_y
k_x
10 rad/um
(c)
(nm)
130
91
52
14
-25
10 μm
(d)
$\times 10^5$
$\sigma = 1.13$ nm
Count
Background Noise (nm)

3.

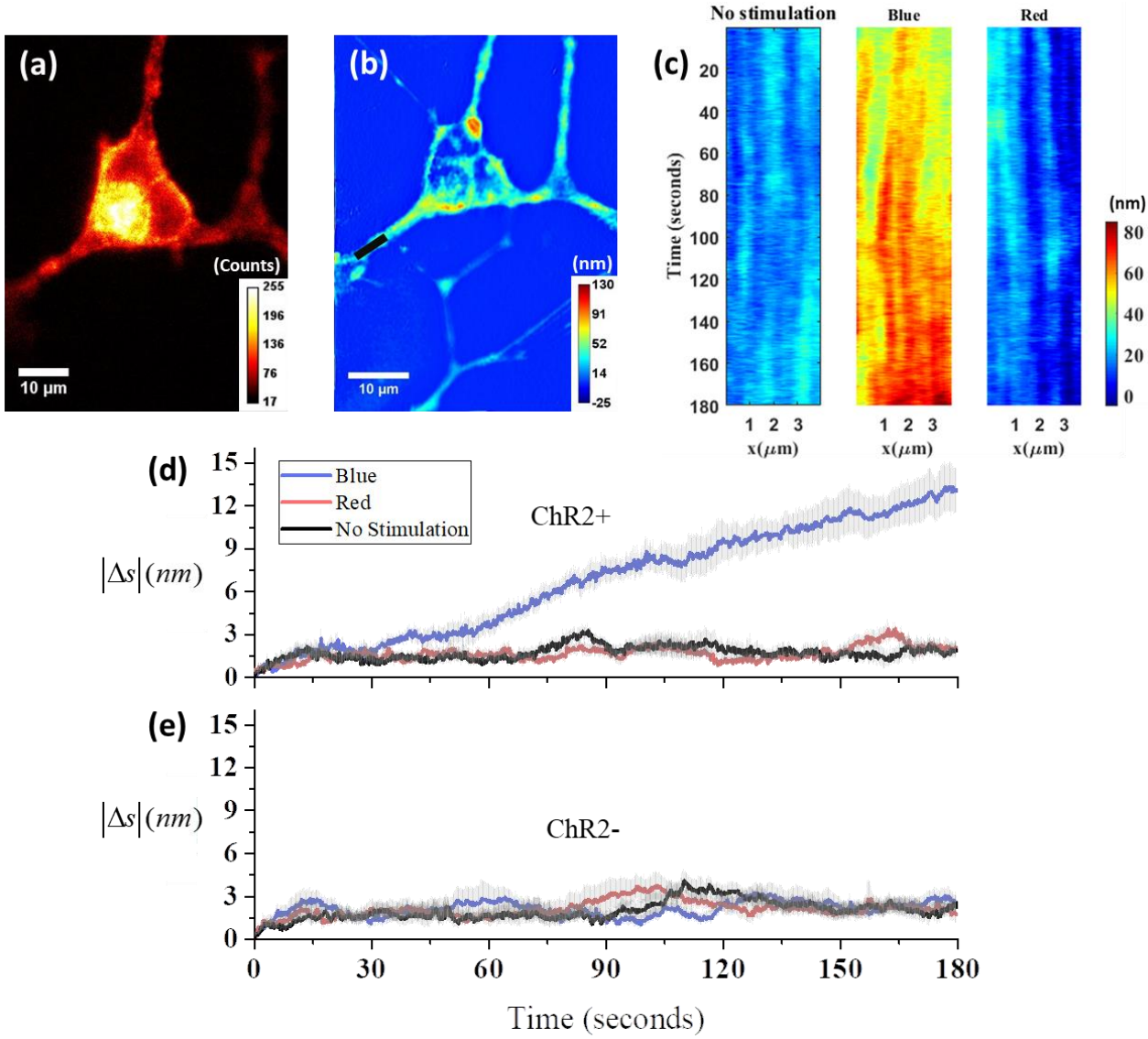
(a)
(Counts)
255
196
136
76
17
10 µm
(b)
(nm)
130
91
52
14
-25
10 µm
(c)
No stimulation
Blue
Red
Time (seconds)
20
40
60
80
100
120
140
160
180
1 2 3
x(µm)
(nm)
80
60
40
20
0
(d)
Blue
Red
No Stimulation
ChR2+
|Δs|(nm)
15
12
9
6
3
0
(e)
ChR2-
|Δs|(nm)
0
30
60
90
120
150
180
Time (seconds)

4.

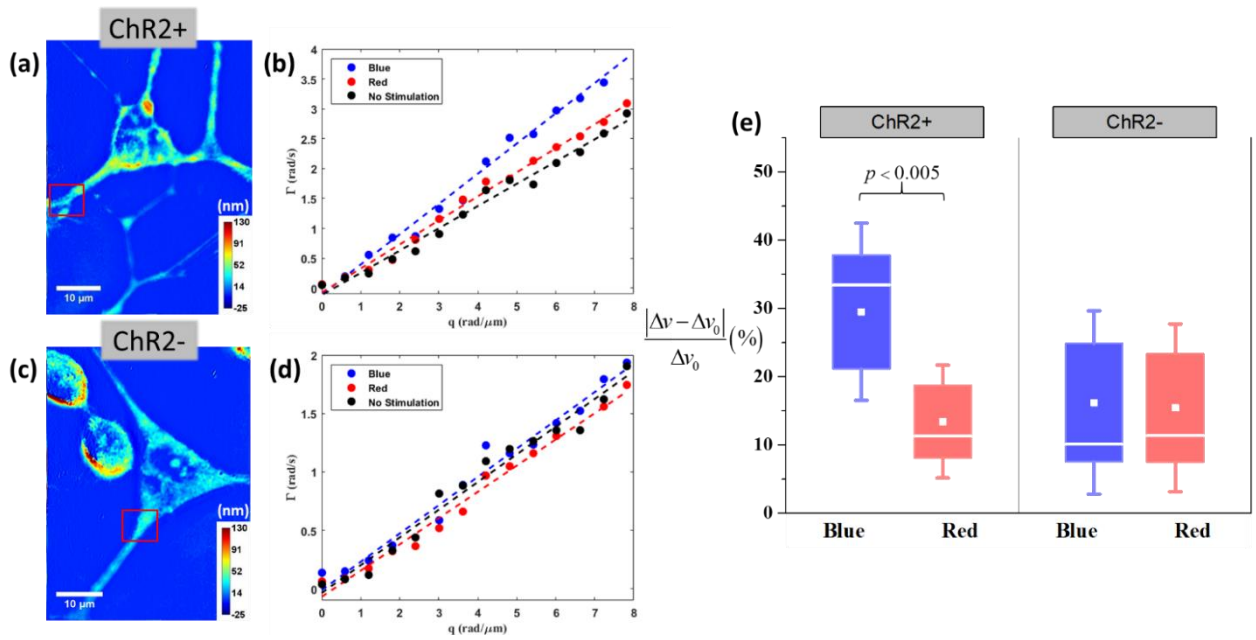
ChR2+
(a)
(nm)
130
91
52
14
-25
10 μm
(b)
Blue
Red
No Stimulation
Γ (rad/s)
q (rad/μm)
ChR2-
(c)
(nm)
130
91
52
14
-25
10 μm
(d)
Blue
Red
No Stimulation
Γ (rad/s)
q (rad/μm)
(e)
ChR2+
ChR2-
p < 0.005
$\frac{|\Delta v - \Delta v_0|}{\Delta v_0}$ (%)
Blue
Red
Blue
Red

5.

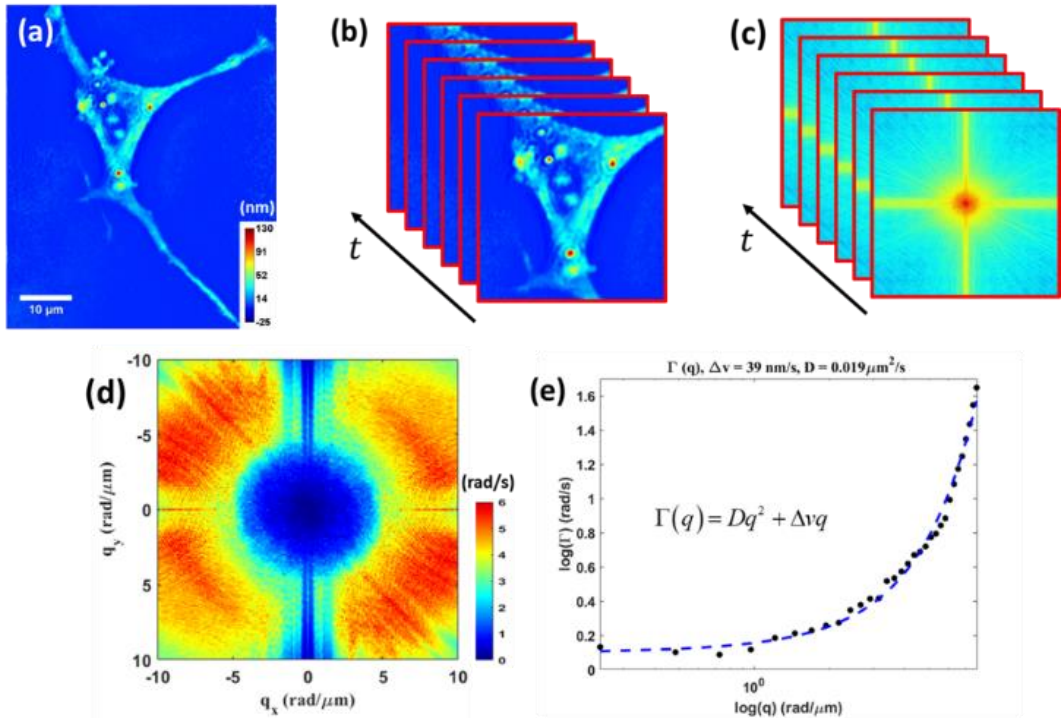
(a)
(nm)
130
91
52
14
-25
10 μm
(b)
t
(c)
t
(d)
(rad/s)
q_y (rad/μm)
q_x (rad/μm)
(e)
Γ (q), Δv = 39 nm/s, D = 0.019μm²/s
$\Gamma(q) = Dq^2 + \Delta v q$
log(Γ) (rad/s)
log(q) (rad/μm)